**ORIGINAL**

**Junguo Wang · Jianzhong Zhou · Dawei Dong · Bin Yan ·
Chunrong Huang**

# Nonlinear dynamic analysis of a rub-impact rotor supported by oil film bearings

**Abstract**  A general model of a rub-impact rotor system is set up and supported by oil film journal bearings. The Jacobian matrix of the system response is used to calculate the Floquet multipliers, and the stability of periodic response is determined via the Floquet theory. The nonlinear dynamic characteristics of the system are investigated when the rotating speed and damping ratio is used as control parameter. The analysis methods are inclusive of bifurcation diagrams, Poincaré maps, phase plane portraits, power spectrums, and vibration responses of the rotor center and bearing center. The analysis reveals a complex dynamic behavior comprising periodic, multi-periodic, chaotic, and quasi-periodic response. The modeling results thus obtained by using the proposed method will contribute to understanding and controlling of the nonlinear dynamic behaviors of the rotor-bearing system.

**Keywords**  Nonlinear dynamics · Chaos · Bifurcation · Rub-impact · Stability

## 1 Introduction

The rub-impact of rotor-to-stator often occurs in high-speed rotating machinery such as turbine generator, hydraulic motor, centrifugal compressor, and aerospace motor. The subsequent rubbing at the contact area may lead to the shutdown of a motor; the rubbing between a blade and its seals could result in serious malfunction and catastrophic failure. On the other hand, rotor-to-stator rub is also a secondary effect that is caused by some other malfunctions such as excessive unbalance, rotor bow, and self-excited instability of the rotor system; thus, the consideration of rub impact of the dynamic analysis has become more and more important.

Since the rotor-stator rub is one of the main faults for large rotary machines, the mechanisms and dynamic behaviors of rub-impact have been widely discussed by many researchers. Ehrich [1] studied the bifurcation of a bearing-rotor system identifying a sub-harmonic vibration phenomenon in a rotor system by means of a simple model of a Jeffcott rotor. He noted that the vibratory response in the transition zone midway between adjacent zones of sub-harmonic response had all the characteristics of chaotic behavior. Li and Paidoussis [2] proposed a new model for a shaver rotor-casing system with clearance and mass imbalance. They developed the Lyapunov exponent technique so as to characterize the topologically different behavior. The effect was illustrated by phase plots, bifurcation diagrams, and Poincaré maps. Muszynska and Goldman [3] performed an experiment of unbalanced rotor/bearing/stator systems with rubbing. The vibration behavior of the systems was characterized by orderly harmonic and sub-harmonic responses,

J. Wang (✉) · D. Dong · B. Yan · C. Huang
School of Mechanical Engineering, Southwest Jiaotong University, Chengdu 610031, Sichuan, China
E-mail: jg_wang2000@163.com

J. Zhou
College of Hydropower and Information Engineering, Huazhong University of Science and Technology, Wuhan 430074, China

as well as by chaotic patterns of vibrations. All results substantiated the fact that chaotic vibration zones decreased with increasing damping. G. Adiletta et al. [4] analyzed the dynamic of a rigid rotor system supported on plain journal bearings. The investigation was supported by the harmonic analysis and the examination of the orbits covered by three assigned points along the rotor axis. They proved the motion of a rotor operating with considerable values of the static eccentricity in any case. Chu and Zhang [5] made an investigation of vibration characteristics of a rub-impact rotor which included nonlinear rub-impact forces resulting from eccentric rotation. When the rotating speed was increased, they found that the grazing bifurcation, the quasi-periodic motion, and chaos occurred after the rub-impact. Meantime, they proved the evidence that damping can effectively suppress chaotic vibration and reduce vibration amplitude. Dai et al. [6] designed an experiment involving rotor-stop rubbing and analyzed its vibration responses. The experiment showed that the full rubbing occurred with serious continuous friction when the amplitude of the excitation force exceeded a certain value. Lu et al. [7] discussed the existence of rub-impact periodic motions in an eccentric rotor system and analyzed a criterion for the periodicity condition or other conditions for real rub-impacts. Some results were obtained by theoretical analyses, including the existence of grazing circle motions and that of single-impact periodic motions. Chu and Lu [8] investigated the nonlinear vibration of a rub-impact rotor system and observed a variety of periodic motions. The vibration waveforms, orbits, and Poincaré maps were applied to analyze nonlinear responses and bifurcation characteristics when the rub-impact occurred. It was concluded that the system motion generally contained multiple harmonic components.

To get the most accurate solutions of the nonlinear dynamics for the flexible rotor system and use it in practice, there have been much more researches over the past five years. Luo et al. [9] induced a crack and rub-impact model for the rotor-bearing system. They used the shooting algorithm for periodic solution and found different bifurcation forms such as saddle-node bifurcation, periodic- doubling bifurcation, and the Hopf bifurcation in the system. Shen et al. [10] introduced a general model of a rub-impact rotor-bearing system with initial permanent bow. The rubbing model was assumed to consist of the radial elastic impact and the tangential Coulomb type of friction. Results showed different motion styles such as periodic, quasi-periodic and even chaotic vibrations. Yuan et al. [11] analyzed nonlinear dynamic behaviors of rotor's radial rub-impact in the presence of turbo- rotor's clearance-excitation force. They observed much more complicated dynamic behaviors with the help of bifurcation diagrams, frequency spectrums, Poincare maps, and frequency waterfalls. Zhang et al. [12] presented a rub-impact micro-rotor mode and investigated the nonlinear dynamic characteristics in micro-electro-mechanical systems (MEMS) when the rotating speed, imbalance, damping coefficient, scale length, and fractal dimension were regarded as the control parameters. They found the effects of these parameters on the micro-rotor system responses. Chang-Jian et al. [13] discussed the dynamic trajectories of rub-impact rotor supported by turbulent journal bearings and lubricated with couple stress fluid under quadratic damping. The phase plane portraits, power spectrum, and Lyapunov exponent were applied to analyze the dynamic behavior. Results revealed that the motions with different speed ratios exhibited as periodic, quasi-periodic, and chaotic types. They also [14] made a detailed analysis of rub-impact rotor system supported by stress fluid film journal bearings. The nonlinear fluid film force, rub-impact force, and nonlinear suspension were applied to the system. It was concluded that couple stress fluid used to be lubricant can improve dynamics of rotor-bearing system. Wang [15] developed a model of the rotor center and journal center of the flexible rotor supported by relative short spherical gas bearing. Numerical calculation revealed the complex dynamic behavior comprising periodic, sub-harmonic, quasi-periodic, and chaotic responses of the rotor-journal system. Khanlo et al. [16] conducted an investigation of the rotating continuous flexible shaft-rigid disk system with rub-impact between the disk and stator. The proposed method was used to discretize the partial differential equations of motion, and the research confirmed that the rub-impact occurred at lower speed ratios owing to the Coriolis and centrifugal forcing effect.

Owing to the above researches, we think that the nonlinear dynamic analysis of rotor-bearing system should take the rub-impact force and oil film force into consideration. In this paper, attention is paid to the nonlinear analysis of the unsteady oil film rotor-bearing system with a nonlinear oil film force. The dynamic model of rotor-bearing systems with rub-impact is established, and the complex nonlinear dynamic phenomena of the system are discussed along with the change of the rotating speed. Some behaviors curves of different parameters on the nonlinear dynamic properties, such as bifurcation diagrams, phase plane portraits, Poincare maps, spectrum analysis diagrams, and time sequence response diagrams of the system, are gained. And nonlinear chaos behaviors of the system are also discovered.
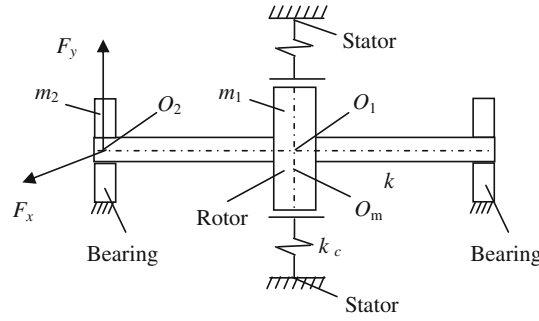
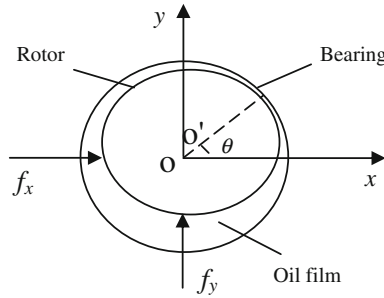**Fig. 1** Schematic of the rub-impact rotor system



**Fig. 2** Cross section schematic of the oil film bearing

## 2 Physical model and governing equations

### 2.1 Oil film forces of the bearing

The model discussed is a Jeffcott rotor supported on identical oil film bearings at both sides as shown in Fig. 1, $O_1$ and $O_2$ are the geometric center of the disk and the journal, $O_m$ is the mass center of the disk with the eccentricity $e$ from $O_1$. To analyze the rotor-bearing system, it makes some assumptions that axial and torsional vibrations are negligible, and the transverse vibration of rotor system is taken into account.

Figure 2 shows the schematic of oil film bearing. Considering the nonlinear oil film force model under the short bearing theory, the dynamic turbulent Reynolds equation for the pressure $p$ in the lubricating film is [17]:

$$\left(\frac{R}{L}\right)^2 \frac{\partial}{\partial z}\left(h^3 \frac{\partial p}{\partial z}\right) = x\sin\theta - y\cos\theta - 2\left(x'\cos\theta + y'\sin\theta\right), \tag{1}$$

$L$ is the length of the bearing, $R$ is the radius of the bearing, $h$ represents the oil film thickness, $z$ is the non-dimensional axial displacement of the journal center. Integrating Eq. (1), the distribution of oil film pressure is obtained

$$p = \frac{1}{8}\left(\frac{L}{R}\right)^2 \frac{(x - 2y')\sin\theta - (y + 2x')\cos\theta}{(1 - x\cos\theta - y\sin\theta)^3}\left(4z^2 - 1\right). \tag{2}$$

Equation (2) is written in the hypothesis of zero relative pressure of the lubricant in the cavitated zone and on both sides of the bearing. The extension of the lubricating film is assumed corresponding to the interval $[\alpha, \alpha + \pi]$ of the angular co-ordinate $\theta$, and the angle $\alpha$ is defined by means of the expression

$$\alpha = \arctan\frac{y + 2x'}{x - 2y'} - \frac{\pi}{2}\text{sign}\left(\frac{y + 2x'}{x - 2y'}\right) - \frac{\pi}{2}\text{sign}\left(y + 2x'\right). \tag{3}$$

The dimensionless components of the fluid film force is given the following expressions, obtained with Eq. (2) through integration along the lubricated arc of bearing

$$\left\{\begin{matrix} f_x \\ f_y \end{matrix}\right\} = \frac{1}{\sigma P}\left\{\begin{matrix} F_x \\ F_y \end{matrix}\right\} = 2\int_{\alpha}^{\alpha+\pi}\frac{(x - 2y')\sin\theta - (y + 2x')\cos\theta}{(1 - x\cos\theta - y\sin\theta)^3}\left\{\begin{matrix} \cos\theta \\ \sin\theta \end{matrix}\right\}d\theta \tag{4}$$

The solution for $f_x$ and $f_y$ is based on the following integrals:

$$I_1(x, y, \alpha) = \int\limits_{\alpha}^{\alpha+\pi} \frac{\cos^2 \theta}{(1 - x \cos \theta - y \sin \theta)^3} d\theta$$

$$I_2(x, y, \alpha) = \int\limits_{\alpha}^{\alpha+\pi} \frac{\sin^2 \theta}{(1 - x \cos \theta - y \sin \theta)^3} d\theta \tag{5}$$

$$I_3(x, y, \alpha) = \int\limits_{\alpha}^{\alpha+\pi} \frac{\sin \theta \cos \theta}{(1 - x \cos \theta - y \sin \theta)^3} d\theta$$

A numerical solution of these integrals can be avoided adopting the relationships

$$G(x, y, \alpha) = \int\limits_{\alpha}^{\alpha+\pi} \frac{d\theta}{1 - x \cos \theta - y \sin \theta}$$

$$= \frac{2}{(1-x^2-y^2)^{1/2}} \left[ \frac{\pi}{2} + \arctan \frac{y \cos \alpha - x \sin \alpha}{(1-x^2-y^2)^{1/2}} \right], \tag{6}$$

$$I_1(x, y, \alpha) = \tfrac{1}{2} \tfrac{\partial^2}{\partial x^2} G(x, y, \alpha)$$

$$I_2(x, y, \alpha) = \tfrac{1}{2} \tfrac{\partial^2}{\partial y^2} G(x, y, \alpha)$$

$$I_3(x, y, \alpha) = \frac{1}{2} \frac{\partial^2}{\partial x \partial y} G(x, y, \alpha). \tag{7}$$

By means of Eqs. (6) and (7), from the expression Eq. (3), it follows

$$\left\{ \begin{array}{c} f_x \\ f_y \end{array} \right\} = \left\{ \begin{array}{c} (x - 2y') \frac{\partial^2 G}{\partial x \partial y} - (y + 2x') \frac{\partial^2 G}{\partial x^2} \\ (x - 2y') \frac{\partial^2 G}{\partial y^2} - (y + 2x') \frac{\partial^2 G}{\partial x \partial x} \end{array} \right\}. \tag{8}$$

The eventual expression of non-dimensional oil film force can be written as

$$\left\{ \begin{array}{c} f_x \\ f_y \end{array} \right\} = -\frac{\left[ (x - 2y')^2 + (y + 2x')^2 \right]^{1/2}}{1 - x^2 - y^2} \times \left\{ \begin{array}{c} 3x V(x, y, \alpha) - \sin \alpha G(x, y, \alpha) - 2 \cos \alpha S(x, y, \alpha) \\ 3y V(x, y, \alpha) - \cos \alpha G(x, y, \alpha) - 2 \sin \alpha S(x, y, \alpha) \end{array} \right\}, \tag{9}$$

where

$$V(x, y, \alpha) = \frac{2 + (y \cos \alpha - x \sin \alpha) G(x, y, \alpha)}{1 - x^2 - y^2}, \tag{10}$$

$$S(x, y, \alpha) = \frac{x \cos \alpha + y \sin \alpha}{1 - (x \cos \alpha + y \sin \alpha)^2}, \tag{11}$$

$$G(x, y, \alpha) = \frac{2}{(1 - x^2 - y^2)^{1/2}} \left[ \frac{\pi}{2} + \arctan \frac{y \cos \alpha - x \sin \alpha}{(1 - x^2 - y^2)^{1/2}} \right], \tag{12}$$

## 2.2 Rub-impact force

It is assumed that there is an initial clearance of $\delta$ between the rotor and stator, and the rotational speed of rotor is $\omega$. The rubbing model is shown in Fig. 3. From the above assumptions, the radial impact force $F_N$ and the tangential rub force $F_T$ could be expressed as

$$F_N(x, y) = \begin{cases} 0 & (\text{for} \quad e < \delta), \\ (e - \delta) k_c & (\text{for} \quad e \geq \delta), \end{cases} \quad F_T = f F_N, \tag{13}$$

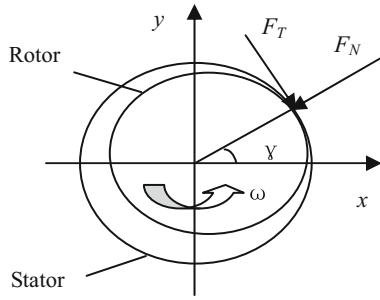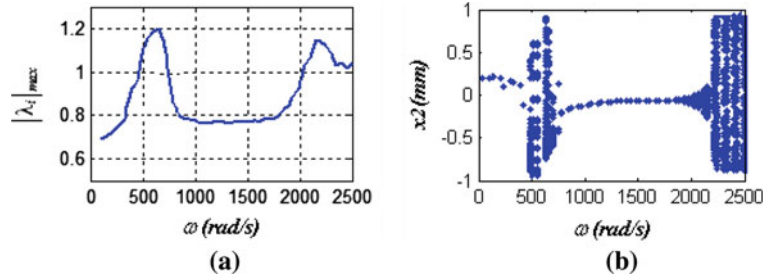**Fig. 3** Schematic of rub and impact forces



**Fig. 4** Change diagram of the Floquet multiplier and bifurcation diagram of the bearing center. **a** Change of the Floquet multipliers. **b** Bifurcation diagram of bearing center
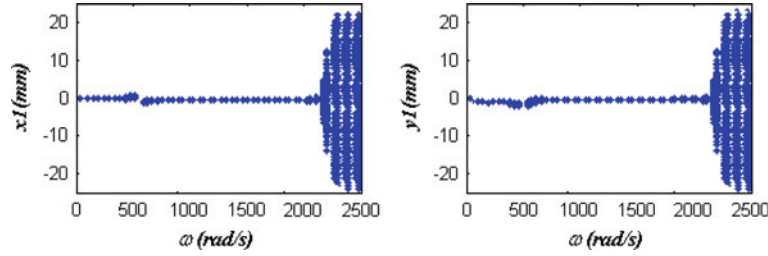


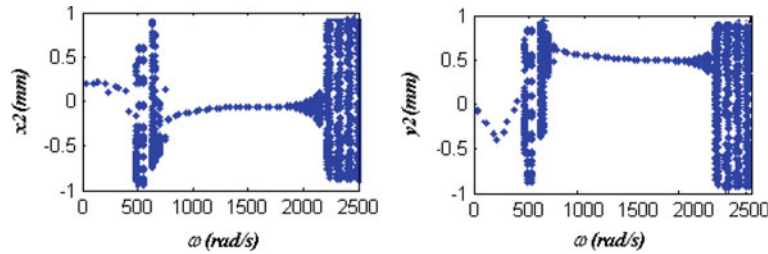**Fig. 5** Bifurcation diagrams of rotor center with the rotating speed as the control parameter
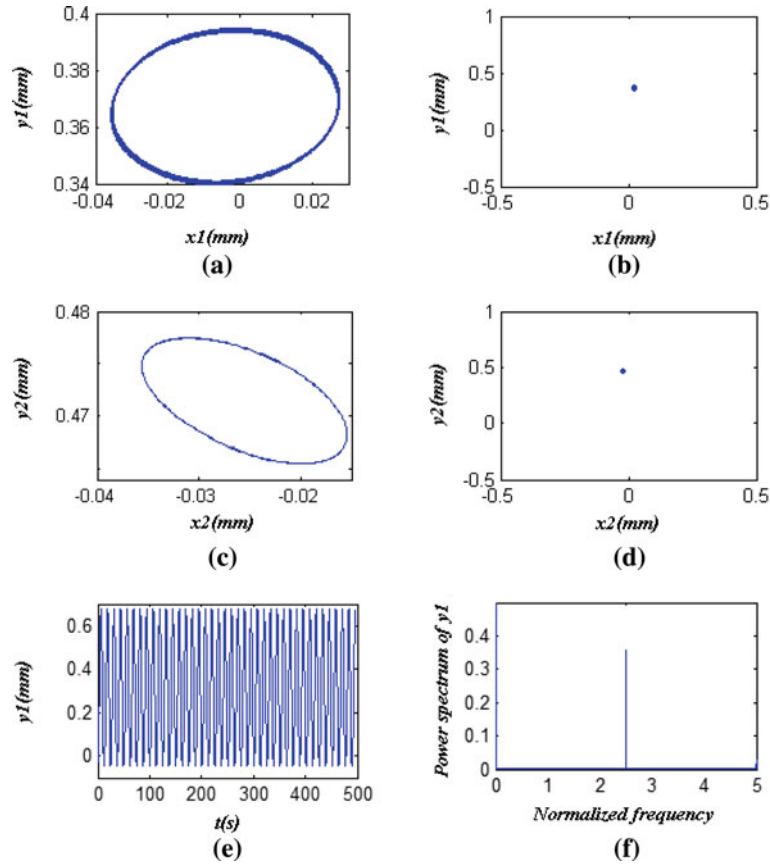


**Fig. 6** Bifurcation diagrams of bearing center with the rotating speed as the control parameter

where $e = \sqrt{x^2 + y^2}$ is the radial displacement of the rotor, $f$ is the friction coefficient between rotor and stator, $k_c$ is radial stiffness of the stator. When rub-impact happens, the rub-impact forces can be written in $x - y$ co-ordinates as [5]

$$F_x(x, y) = -F_N \cos \gamma + F_T \sin \gamma,$$
$$F_Y(x, y) = -F_N \sin \gamma - F_T \cos \gamma. \tag{14}$$

Substitution of Eq. (13) into Eq. (14) gives

$$\left\{ \begin{array}{c} F_x \\ F_y \end{array} \right\} = -H(e - \delta) \frac{(e - \delta)}{e} \left[ \begin{array}{cc} 1 & -f \\ f & 1 \end{array} \right] \left\{ \begin{array}{c} x \\ y \end{array} \right\} \tag{15}$$

**Fig. 7** Phase plane portrait and Poincaré map of rotor center and bearing center at $\omega = 400$. **a** Phase plane portrait of rotor center. **b** Poincaré map of rotor center. **c** Phase plane portrait of bearing center. **d** Poincaré map of bearing center. **e** Vibration response of rotor center. **f** Power spectrum of rotor center

where

$$H(x) = \begin{cases} 0, & x \leq 0 \\ 1, & x > 0 \end{cases} \tag{16}$$

Equation (15) indicates that when the rotor displacement $e$ is smaller than $\delta$, there will be no rub-impact interaction and the rub-impact forces are zero, else the rub-impacting will happen.

### 2.3 Dynamic equations

It is assumed that $(x_1, y_1)$ and $(x_2, y_2)$ are radial displacements in the disk position and in the bearing position. Taking into account rubbing forces $(F_x, F_y)$ and the oil film forces $(f_x, f_y)$, the equation for the system can be written as

$$\begin{aligned} m_1 \ddot{x}_1 + c_1 \dot{x}_1 + k(x_1 - x_2) &= F_x + m_2 u \omega^2 \cos(\omega t), \\ m_1 \ddot{y}_1 + c_1 \dot{y}_1 + k(y_1 - y_2) &= F_y + m_2 u \omega^2 \sin(\omega t) - m_1 g, \\ m_2 \ddot{x}_2 + c_2 \dot{x}_2 + 2k(x_2 - x_1) &= f_x, \\ m_2 \ddot{y}_2 + c_2 \dot{y}_2 + 2k(y_2 - y_1) &= f_y - m_2 g, \end{aligned} \tag{17}$$

where $m_1$ and $m_2$ are the mass of the disk and the mass of the rotor at the bearing, $c_1$ and $c_2$ are the damping coefficient of rotor at the disk and rotor damping coefficient at the bearing, respectively, $k$ indicates the stiffness coefficient, $u$ represents unbalance, $g$ is the acceleration of gravity.
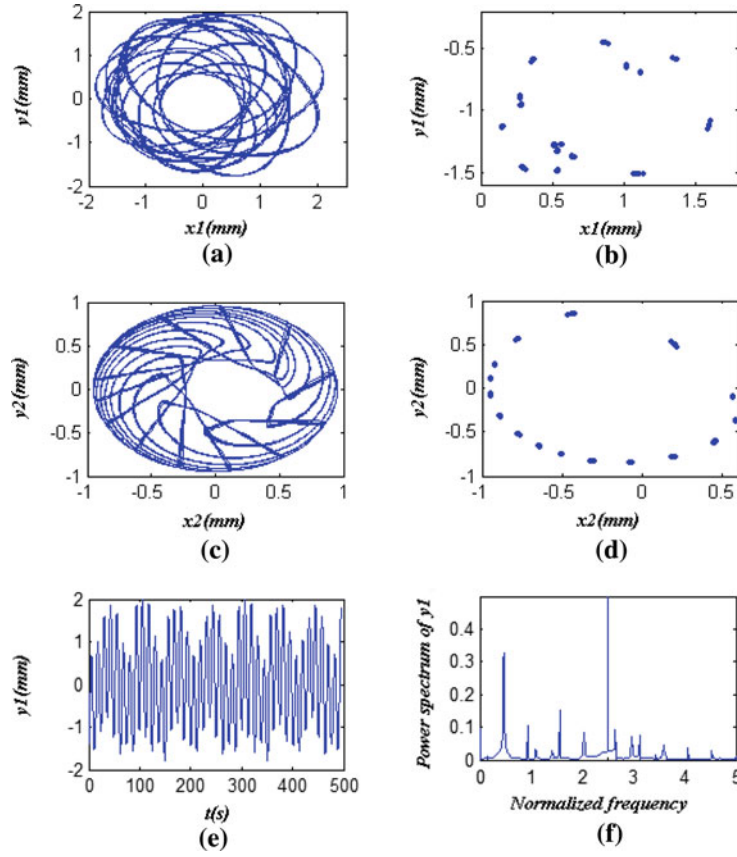
**Fig. 8** Phase plane portrait and Poincaré map of rotor center and bearing center at $\omega = 500$. **a** Phase plane portrait of rotor center. **b** Poincaré map of rotor center. **c** Phase plane portrait of bearing center. **d** Poincaré map of bearing center. **e** Vibration response of rotor center. **f** Power spectrum of rotor center

To give the equations a dimensionless form, it can be initially assumed as below

$$s = \mu\omega RL \left(R/c\right)^2 \left(L/2R\right)^2, \ f_X = f_x/s, \ f_Y = f_y/s,$$
$$Y_1 = y_1/c, \ X_1 = x_1/c, \ Y_2 = y_2/c, \ X_2 = x_2/c, \ \tau = \omega t, \tag{18}$$

$\mu$ is the oil viscosity, and $c$ is the radial clearance of the bearing, then Eq. (17) becomes

$$\ddot{X}_1 = -\frac{c_1}{\omega m_1}\dot{X}_1 - \frac{k}{\omega^2 m_1}(X_1 - X_2) + \frac{F_X(X_1, Y_1)}{c\omega^2 m_1} + \bar{b}\cos\tau,$$
$$\ddot{Y}_1 = -\frac{c_1}{\omega m_1}\dot{Y}_1 - \frac{k}{\omega^2 m_1}(Y_1 - Y_2) + \frac{F_Y(X_1, Y_1)}{c\omega^2 m_1} - \frac{g}{c\omega^2} + \bar{b}\sin\tau,$$
$$\ddot{X}_2 = -\frac{c_2}{\omega m_2}\dot{X}_2 - \frac{2k}{\omega^2 m_2}(X_2 - X_1) + \frac{s}{c\omega^2 m_2}f_X\left(X_2, Y_2, \dot{X}_2, \dot{Y}_2\right),$$
$$\ddot{Y}_2 = -\frac{c_2}{\omega m_2}\dot{Y}_2 - \frac{2k}{\omega^2 m_2}(Y_2 - Y_1) + \frac{s}{c\omega^2 m_1}f_Y\left(X_2, Y_2, \dot{X}_2, \dot{Y}_2\right) - \frac{g}{c\omega^2} \tag{19}$$
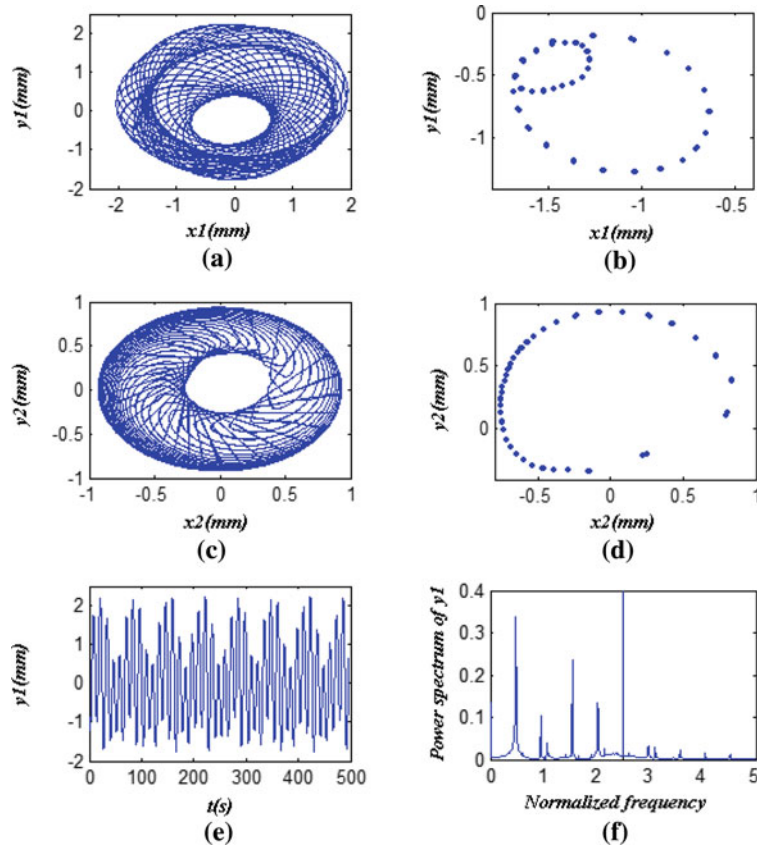
The parameters of the rotor-bearing system used are as follows:

$$m_1 = 35\,\text{kg}, \ m_2 = 4\,\text{kg}, \ R = 0.028\,\text{m}, \ L = 0.013\,\text{m}, \ c = 0.00011\,\text{m},$$
$$\mu = 0.018\,\text{pa s}, \ f = 0.10, \ c_1 = 2100\,\text{N s/m}, \ c_2 = 1050\,\text{N s/m}, \tag{20}$$
$$e = 0.0008\,\text{m}, \ k = 2.5 \times 10^7\,\text{N m}^{-1}, \ k_c = 3.6 \times 10^7\,\text{N m}^{-1}.$$

## 3 Nonlinear bifurcation and stability analysis

The dynamic problem of the proposed system can be summed up the following non-automatic system

$$\dot{X} = F(t, u, X), \ (t, u, X) \in R \times R^m \times R^n, \tag{21}$$

**Fig. 9** Phase plane portrait and Poincaré map of rotor center and bearing center at $\omega = 630$. **a** Phase plane portrait of rotor center. **b** Poincaré map of rotor center. **c** Phase plane portrait of bearing center. **d** Poincaré map of bearing center. **e** Vibration response of rotor center. **f** Power spectrum of rotor center

where X is state vector of system, $\boldsymbol{u}$ is the system parameter, that is, the rotating speed of the rotor, diameter-to-width ratio of the bearing, mass eccentricity and so on. The periodic solution of the dynamic system is transformed as solving stationary point of Poincaré maps and judging stability. Equation (21) can also be written as

$$X_{k+1} = P(X_k, u). \tag{22}$$

The curve of the fixed points is described within the given range of parameter $\boldsymbol{u}$ as follows

$$X = P(X, u). \tag{23}$$

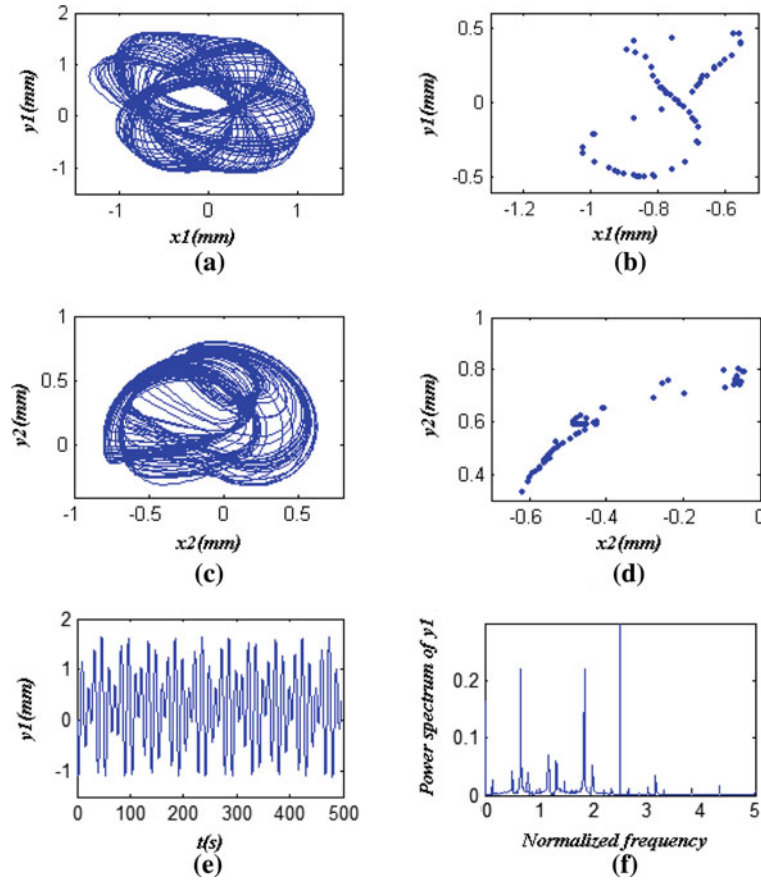Equation (23) can be converted into the following equation

$$H(X, u) = X - P(X, u) = 0. \tag{24}$$

### 3.1 Stability of the solutions

To trace the periodic solutions, the Cauchy form of differential equation is considered and then the following is derived

$$\begin{cases} \dfrac{dX}{du} = -\left[\dfrac{\partial H(X,u)}{\partial X}\right]^{-1} \dfrac{\partial H(X,u)}{\partial u}, \\ X(u_0) = X_0. \end{cases} \tag{25}$$

**Fig. 10** Phase plane portrait and Poincaré map of rotor center and bearing center at $\omega = 700$. **a** Phase plane portrait of rotor center. **b** Poincaré map of rotor center. **c** Phase plane portrait of bearing center. **d** Poincaré map of bearing center. **e** Vibration response of rotor center. **f** Power spectrum of rotor center

Based on the solution at $\boldsymbol{u} = \boldsymbol{u}_n$, a solution can be obtained at $\boldsymbol{u} = \boldsymbol{u}_{n+1}$. Starting from a known solution $X_n$ at $\boldsymbol{u} = \boldsymbol{u}_n$, the prediction of $X_{n+1}$ is

$$\begin{cases} X_{n+1} = X_n - \left[\frac{\partial H(X_n, u_n)}{\partial X}\right]^{-1} \frac{\partial H(X_n, u_n)}{\partial u} \Delta u, \\ u_{n+1} = u_n + \Delta u. \end{cases} \tag{26}$$

The observed states of the system are usually displacement and velocity disturbances of the center of the rotor. In order to trace the periodic solutions curve with change of parameter $\boldsymbol{u}$, the Jacobian $\partial H(X_n, u_n)/\partial X$ and $\partial H(X_n, u_n)/\partial u$ must be found by the observed states at $\boldsymbol{u} = \mathbf{u}_n$.

Taking the partial derivative of Eq. (24) with respect to $X$, the following equation is obtained

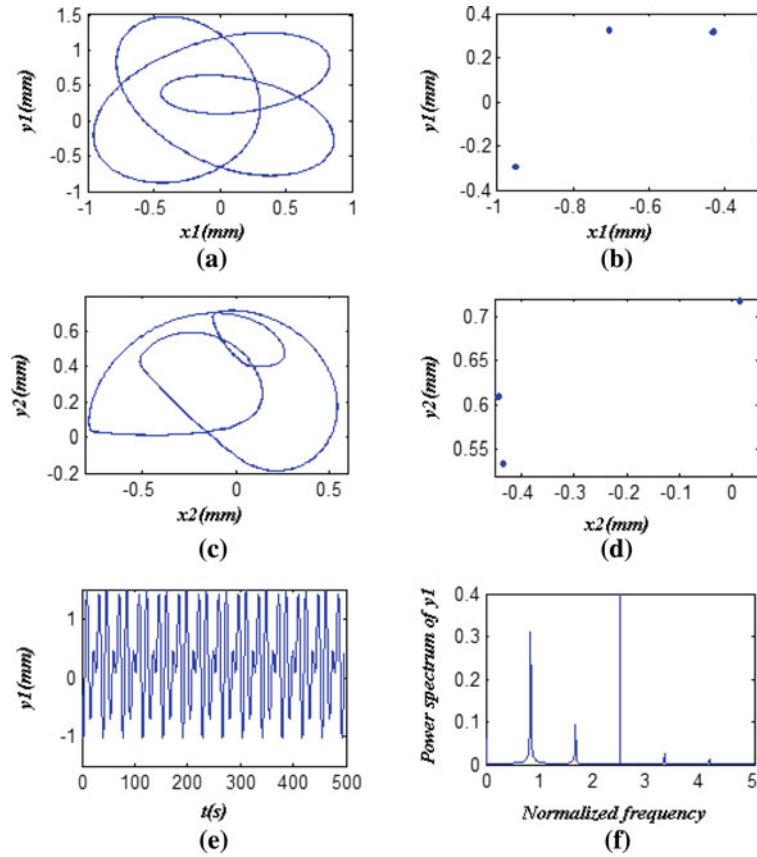$$\frac{\partial H}{\partial X} = I - \frac{\partial P}{\partial X}. \tag{27}$$

Equation (23) is spread at $X = X_n$, only the linear terms being remained, to give the following equation

$$P(X) \approx P(X_n) + \frac{\partial P(X_n)}{\partial X_n}(X - X_n). \tag{28}$$

Substitution of Eq. (28) into Eq. (22) gives

$$X_{k+1} = \frac{\partial P(X_n)}{\partial X} X_k + C_n, \tag{29}$$

where $C_n = P(X_n) - (\partial P(X_n)/\partial X)X_n$ is a constant column vector.

**Fig. 11** Phase plane portrait and Poincaré map of rotor center and bearing center at $\omega = 750$. **a** Phase plane portrait of rotor center. **b** Poincaré map of rotor center. **c** Phase plane portrait of bearing center. **d** Poincaré map of bearing center. **e** Vibration response of rotor center. **f** Power spectrum of rotor center

For a $d$-order system, a series of Poincaré map points left by $X_n$ crossing the Poincaré section at the same direction, that is, $X_k(k = 1, 2, \ldots, d + 1)$ is within a certain neighborhood, Thus, $X_k$ can be written as

$$
\begin{cases}
X_1 = \frac{\partial P(X_n)}{\partial X} X_0 + C_n, \\
X_2 = \frac{\partial P(X_n)}{\partial X} X_1 + C_n, \\
\cdots \\
X_{d+1} = \frac{\partial P(X_n)}{\partial X} X_d + C_n.
\end{cases}
\tag{30}
$$

If $X^{d+1} = [X_1, X_2, \ldots, X_{d+1}]$, $X^d = [X_1, X_2, \ldots, X_d]$, Eq. (29) can be described as

$$
X^{d+1} \approx \left[ \frac{\partial P(X_n)}{\partial X} \quad C_n \right] \cdot \begin{bmatrix} X^d \\ E \end{bmatrix},
\tag{31}
$$
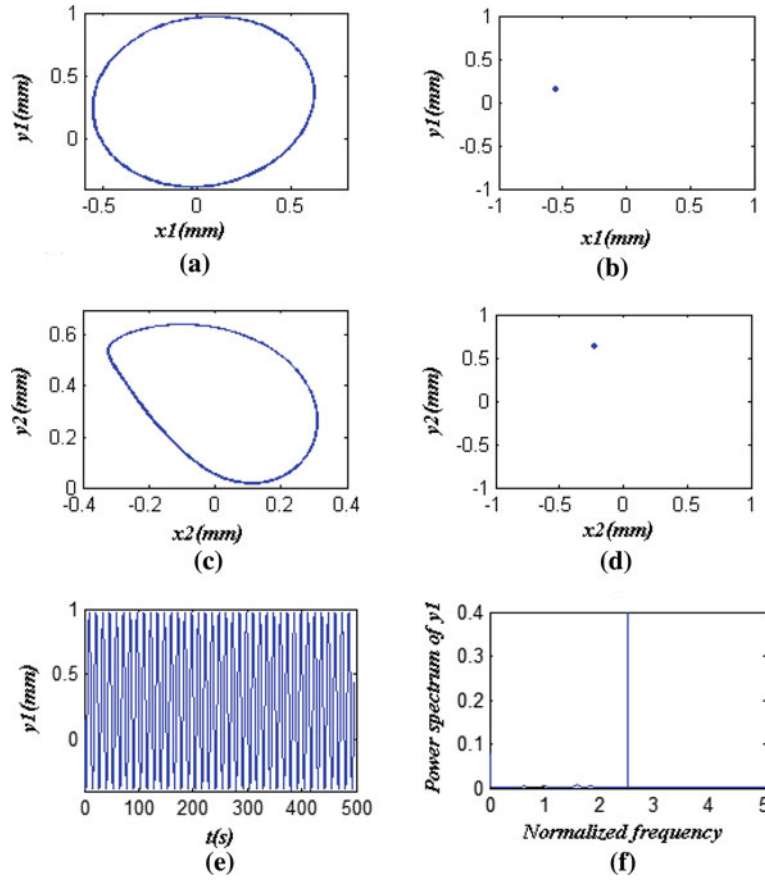
where $E = [1, 1, \ldots, 1]$. From Eq. (31), the following equation is easy to get

$$
\left[ \frac{\partial P(X_n)}{\partial X} \quad C_n \right] = \begin{bmatrix} X^d \\ E \end{bmatrix}^{-1} \cdot X^{d+1}.
\tag{32}
$$

Jacobian $\partial H(X_n, u_n)/\partial X$ can be determined by Eqs. (27) and (32).

It is assumed that $\tilde{X}_n$ is one Poincaré map point located on the Poincaré section after one period of disturbing $X_n$. Built on observed steady-state periodic solution being $X_n$, at $u = u_n$, one can get

$$
\frac{\partial H(X_n, u_n)}{\partial u} = \frac{\tilde{X}_n - X_n}{\Delta u}.
\tag{33}
$$

**Fig. 12** Phase plane portrait and Poincaré map of rotor center and bearing center at $\omega = 800$. **a** Phase plane portrait of rotor center. **b** Poincaré map of rotor center. **c** Phase plane portrait of bearing center. **d** Poincaré map of bearing center. **e** Vibration response of rotor center. **f** Power spectrum of rotor center

When infinitesimal perturbation $\Delta u$ is exerted on $u_n$, i.e., $u = u_n + \Delta u$ the steady-state periodic solution $X_n$, which is located on the Poincaré section, will cross the Poincaré section again after one period. As $\hat{X}_n$ is difficult to be observed in practice, solving the solution of Eq. (33) can be achieved by the following steps.

Jacobian $\partial H(X_{n-1})/\partial X$ and $C_{n-1}$ is calculated at $u = u_{n-1}$. If $u_{n-1}$ is within the neighborhood of $u_n$, one can derive

$$\hat{X}_n \approx \frac{\partial P(X_{n-1})}{\partial X} X_n + C_{n-1}. \tag{34}$$

Jacobian $\partial H(X_n, u_n)/\partial u_n$ can be obtained at $u = u_n$

$$\frac{\partial H(X_n, u_n)}{\partial u_n} = \frac{\partial P(X_{n-1})/\partial x + C_{n-1} - X_n}{u_{n-1} - u_n}. \tag{35}$$

The corresponding characteristic equation satisfies $|\mathbf{J} - \lambda_i \mathbf{I}| = 0$, where the eigenvalue $|\lambda_i|$ of the matrix is called as the Floquet multiplier of the system.

## 3.2 Bifurcation and stability analysis

Stability of periodic motion of the system is determined according to the Floquet theory [18,19]. If the value $u$ is changed, bifurcation of periodic solution and stability of the system are anticipated by the Floquet multipliers. Concerning stability of Eq. (21), there are the following conclusions: (1) When $|\lambda_i| < 1 (i = 1, 2, \ldots, n)$, the stable periodic solution is asymptotically stable. (2) If there is $\lambda_j$ which passes the unit circle outwards
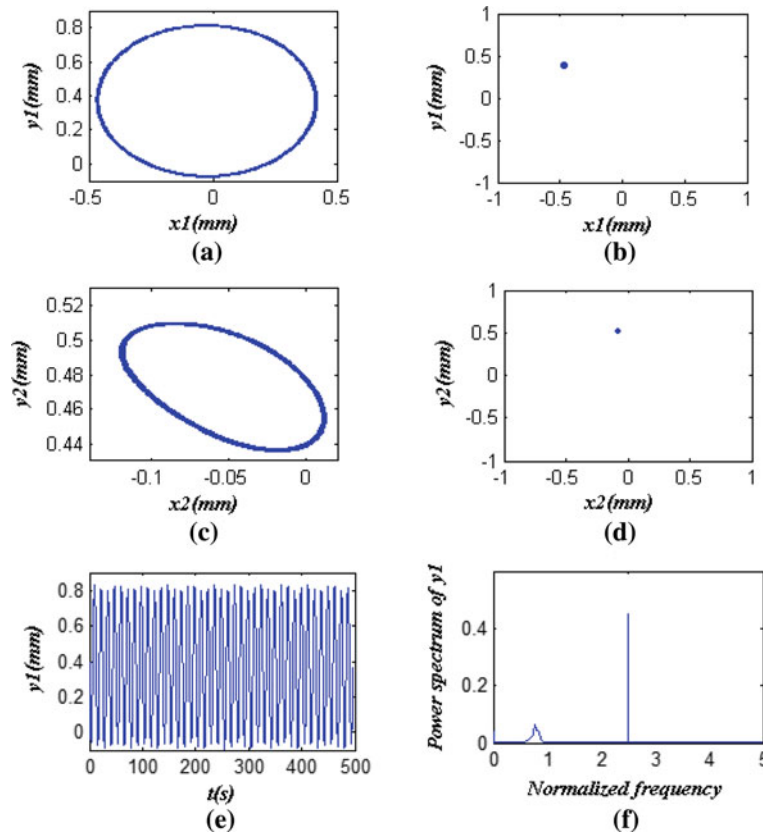
**Fig. 13** Phase plane portrait and Poincaré map of rotor center and bearing center at $\omega = 2,000$. **a** Phase plane portrait of rotor center. **b** Poincaré map of rotor center. **c** Phase plane portrait of bearing center. **d** Poincaré map of bearing center. **e** Vibration response of rotor center. **f** Power spectrum of rotor center

through the point of $-1$ and other $|\lambda_i| < 1 (i = 1, 2, \ldots, n, i \neq j)$, the stable periodic solution will have period-doubling bifurcation. (3) If there is $\lambda_j$ which passes the unit circle outward through the point of $+1$ and other $|\lambda_i| < 1 (i = 1, 2, \ldots, n, i \neq j)$, the stable periodic solution will have the saddle-node bifurcation. (4) If there is a pair of conjugate complex characteristic multipliers $\lambda_j = a \pm jb$ which pass the unit circle outward and other $|\lambda_i| < 1 (i = 1, 2, \ldots, n, i \neq j)$, the stable periodic solution will have the Hopf bifurcation or second Hopf bifurcation, and the bifurcation will lead to an invariant torus. Therefore, the Floquet theory can be applied to judge stability of nonlinear steady-state periodic solutions of Eq. (19). The change diagram of the Floquet multipliers $|\lambda_i|_{\max}$ against the rotating speed of the system is shown in Fig. 4a. It can be seen that when the speed is below 500 rad/s, $|\lambda_i|$ is less than 1, the stable periodic solution is asymptotically stable. But when the rotating speed is changed at the district of (500–790) rad/s, that is, at 700 and 750 rad/s, the Floquet multiplier $|\lambda_i|_{\max}$ is calculated to 1.1502 ($Re(f) = -1.1502$, $Im(f) = 0.0$) and 1.0324 ($Re(f) = -1.0324$, $Im(f) = 0.0$), respectively, the periodic solution crosses the unit circle by $(-1, 0)$, it means that the period-doubling bifurcation occurs. In particular, as the rotating speed is changed from 800 to 2,000 rad/s, $|\lambda_i|$ is less than 1, the system returns to stable state again. Once the speed is greater than 2,000 rad/s, that is, at 2,100 and 2,350 rad/s, the Floquet multiplier $|\lambda_i|_{\max}$ is calculated to be 1.0712 ($Re(f) = -1.0712$, $Im(f) = 0.0$) and 1.0310 ($Re(f) = -1.0310$, $Im(f) = 0.0$), respectively. It is concluded that the stable periodic solution of the system has period-doubling bifurcation according to the Floquet theory.

As an illustration, the bifurcation chart is obtained by Runge–Kutta method with parameters in Eq. (20). As shown in Fig. 4b, when rotating speed is less than 500 rad/s, the motions of the system are stable with period one. But the system shows double periodic bifurcation when the speed is greater than 500 rad/s. In the range from 500 to 790 rad/s of rotating speeds, the motions are in period two and multi-periodic. As the rotating speed is changed from 800 to 2,000, the period-one motion appears again. Once the speed is higher than 2,000 rad/s, the periodic motions tend to lose their stability, and meantime the rotor vibrations will enter double periodic bifurcation motion and quasi-periodic motion.
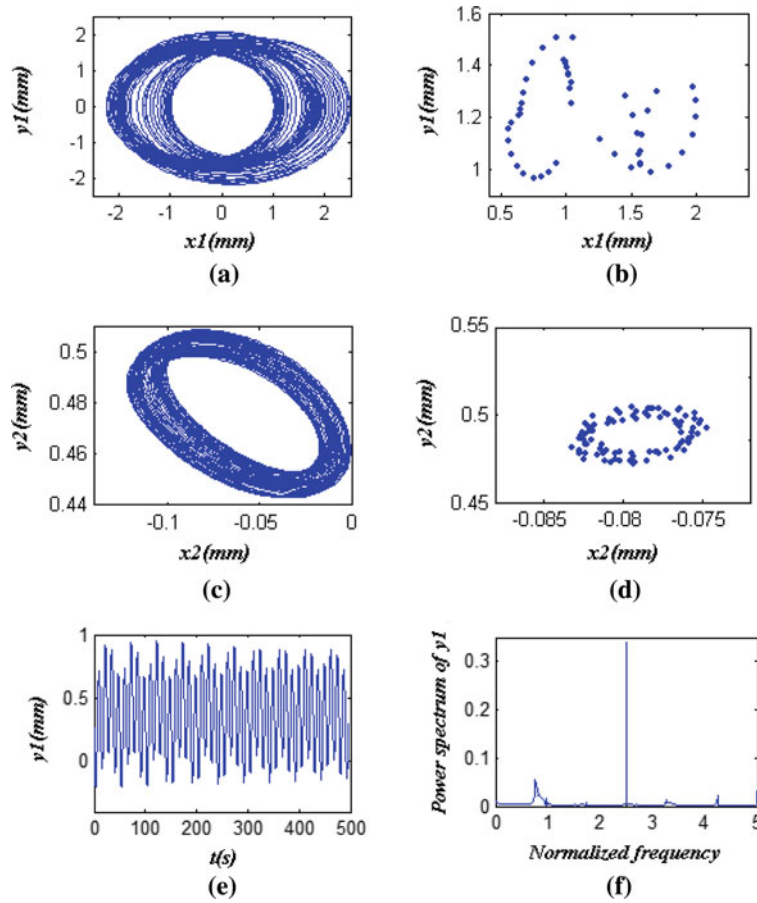
**Fig. 14** Phase plane portrait and Poincaré map of rotor center and bearing center at $\omega = 2{,}050$. **a** Phase plane portrait of rotor center. **b** Poincaré map of rotor center. **c** Phase plane portrait of bearing center. **d** Poincaré map of bearing center. **e** Vibration response of rotor center. **f** Power spectrum of rotor center

## 4 Nonlinear simulation and analysis

### 4.1 Effect of rotating speed

The rotating speed is one of the most important parameters affecting the dynamic characteristics of a rotor system. A bifurcation diagram can provide a summary of the essential dynamics of the system and is therefore a useful way of observing nonlinear dynamic behaviors. Figures 5 and 6 show the bifurcation diagrams of the system in horizontal and vertical direction, using rotating speeds as the control parameter which ranges from 50 to 2,500 rad/s. It is obvious that the response of the system varies with the rotating speed. When the speed is small and less than 500, the dynamic behaviors of bearing center and rotor center are synchronous with period-one motion. Then with the rotor-to-stator rub impact and nonlinear oil film force, the system becomes irregular and enters into the chaotic region at the district of (500–790) rad/s. With the increasing of the rotating speed, the system leaves chaos and comes into period-one motion again between (800, 2,000) rad/s. When the speed is higher than 2,000 rad/s, the system is in complex state, it emerges chaotic motion, period-4 motion, and quasi-periodic motion in sequence.

To further illustrate dynamic behaviors of the system, phase plane portraits, Poincaré maps, power spectrums, and vibration responses are employed. It can be seen that when the speed is less than 500 rad/s., there is a single point in the Poincaré maps, the phase plane portraits are only one closed circle, and the power spectrums also have one-peak amplitude. The results mean that the system response is period-one motion. Meantime, rub-impact phenomenon does not occur as shown in Fig. 7.

When the rotating speed is changed from 500 to 800 rad/s, a series of period-doubling bifurcations occur as the control parameter is increased before entering the chaos regime. Then, a series of period-doubling
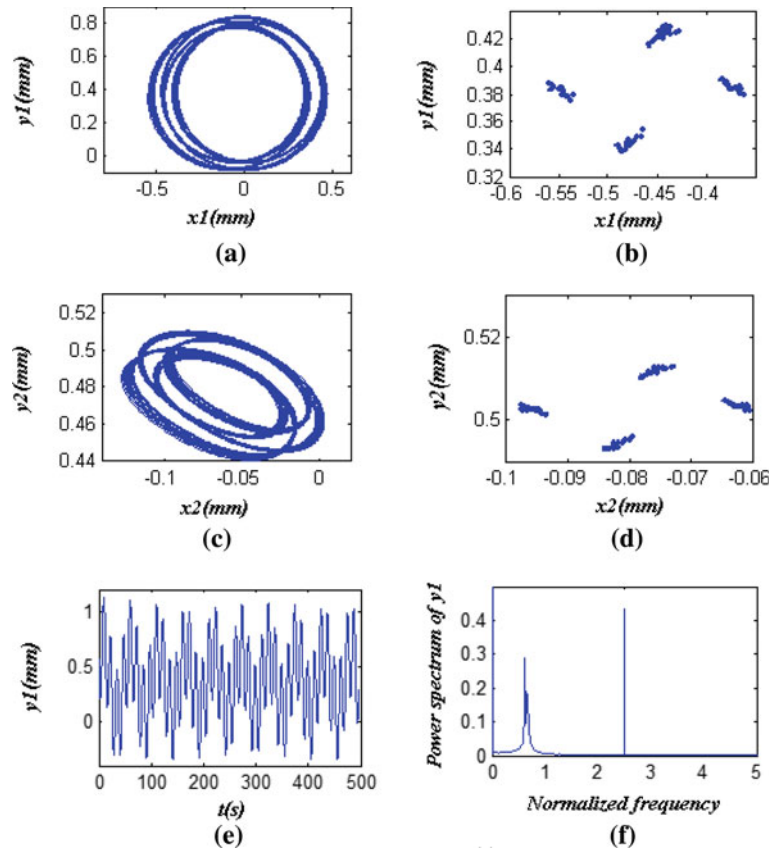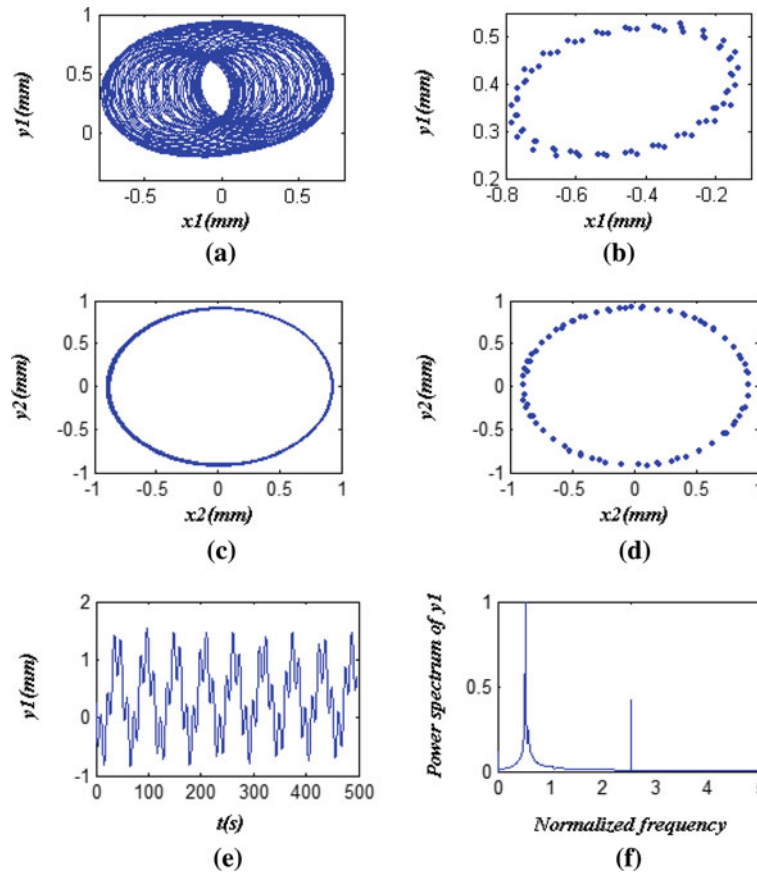
**Fig. 15** Phase plane portrait and Poincaré map of rotor center and bearing center at $\omega = 2{,}250$. **a** Phase plane portrait of rotor center. **b** Poincaré map of rotor center. **c** Phase plane portrait of bearing center. **d** Poincaré map of bearing center. **e** Vibration response of rotor center. **f** Power spectrum of rotor center

bifurcations occur until the limit motion with period one. As shown in Fig. 8, when the speed is equal to 500 rad/s, the power spectral function is broadened, there are sixteen single points in the Poincaré maps, and the phase plane portraits also have sixteen closed circle, indicating that the system is at a period-16 motion. When the speed is changed from 630 to 700 rad/s, phase plane portraits are disorder, the Poincaré maps show many discrete points, and the power spectrum is continuous (Figs. 9, 10). Especially at 700 rad/s, the rotor-stator rub happens, and the Poincaré maps show a special cipher "8" appreciatively. All these results reveal that the system is in state of chaos in this district. In particular, when the speed changes from 710 to 790 rad/s, it happens the so-called "period-3" phenomenon. As displayed in Fig. 11, the phase plane portraits are three closed circle, and also the Poincaré maps have three single points. It can be seen that the system responses contain periodic and chaotic motion alternately at the interval of $500 < \omega < 790$ rad/s.

With the speed near 800 rad/s, however, chaotic vibration disappears, the periodic solutions of the system become stable. As illustrated in Fig. 12, there is a discrete frequency component in the frequency spectrum, and the dynamic response of the system enters period-1 no-rub-impact motion again. Along with the increase of rotating speed, the characteristics of the period-one motion will be displayed, and it keeps the state for a long range of rotating speed until 2,000 rad/s as shown in Figs. 12 and 13.

When the rotating speed continues to increase, the system leaves period-one motion and becomes unstable. As the speed exceeds 2,050 rad/s, rub-impact phenomenon occurs. With the nonlinear oil film force, the changes of the system responses become very complex, that is, at 2,050 rad/s, the return points in the Poincaré maps form a geometrically fractal structure and power spectrum has a broadband. According to these results shown in Fig. 14, the system is in chaotic motion.

From about 2,250 rad/s, the system motion leaves chaos and comes into period-4 motion with four isolated points in Poincaré maps and four circles in the phase plane portraits. Figure 15 indicates that the motion is a sub-synchronous vibration with period-4. When the speed is equal to 2,500 rad/s, there exist two discrete

**Fig. 16** Phase plane portrait and Poincaré map of rotor center and bearing center at $\omega = 2,500$. **a** Phase plane portrait of rotor center. **b** Poincaré map of rotor center. **c** Phase plane portrait of bearing center. **d** Poincaré map of bearing center. **e** Vibration response of rotor center. **f** Power spectrum of rotor center

frequency components in the frequency spectrum as shown in Fig. 16, the phase plane portraits are regular and the Poincaré maps have closed curve. These results also prove that the quasi-periodic motion appears in the system.

### 4.2 Effect of damping

Because of the existence of damping, the rotor-bearing system is a dissipation system from the physical viewpoint. For convenience, taking the damping ratio $\xi = c_1/(2\sqrt{m_1 k})$ as control parameter, the bifurcation diagrams of the rotor system are obtained when the damping ratio $\xi$ is changed from 0.01 to 0.70, where the other parameters for the computation are the same as Eq. (20). As illustrated in Fig. 17, the dynamic responses in the horizontal and vertical direction are almost same, and the response of the rotor system undergoes a complete process from chaos through quasi-periodic motion to period-one motion with the rotating speed equals 1,000 rad/s.

For various damping ratios, the influence of damping on the rotor's dynamics has been studied for three cases; the phase plane portraits and Poincare maps of the system are shown in Figs. 18, 19, and 20.

When the value of damping ratio is equal to 0.13, the phase plane portraits infinitely loop in the enclosed area, but never duplicates. At the same time, the return points in the Poincaré maps form a geometrically fractal structure as displayed in Fig. 18. All of these indicate that the system response is chaotic motion. With the increasing of damping ratio, that is, the damping ratio reaches 0.25, the phase plane portraits become regular, and the attractors of the Poincare maps have closed curve. It is evident that the system is in quasi-periodic motion according to these results shown in Fig. 19. When the damping ratio continues to increase, the points
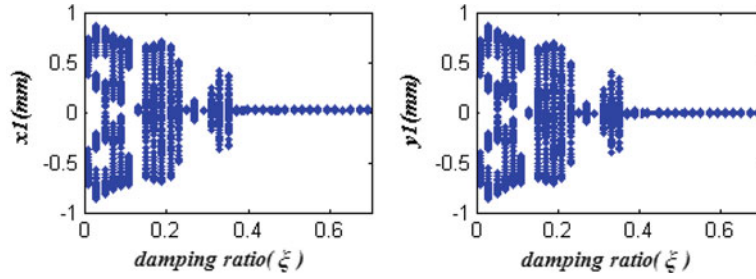
**Fig. 17** The bifurcation diagrams of rotor center with damping ratio as the control parameter
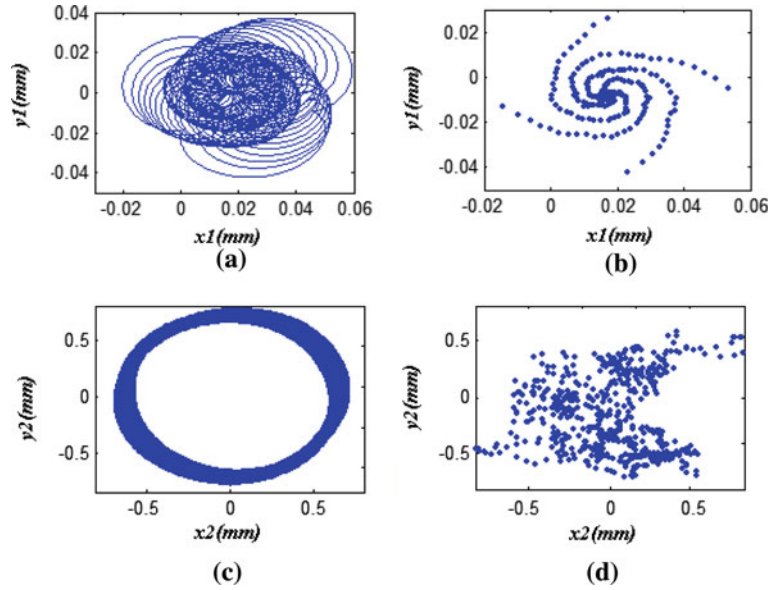


**Fig. 18** Phase plane portrait and Poincaré map of rotor center and bearing center at $\xi = 0.13$. **a** Phase plane portrait of rotor center. **b** Poincaré map of rotor center. **c** Phase plane portrait of bearing center. **d** Poincaré map of bearing center



**Fig. 19** Phase plane portrait and Poincaré map of rotor center and bearing center at $\xi = 0.25$. **a** Phase plane portrait of rotor center. **b** Poincaré map of rotor center. **c** Phase plane portrait of bearing center. **d** Poincaré map of bearing center
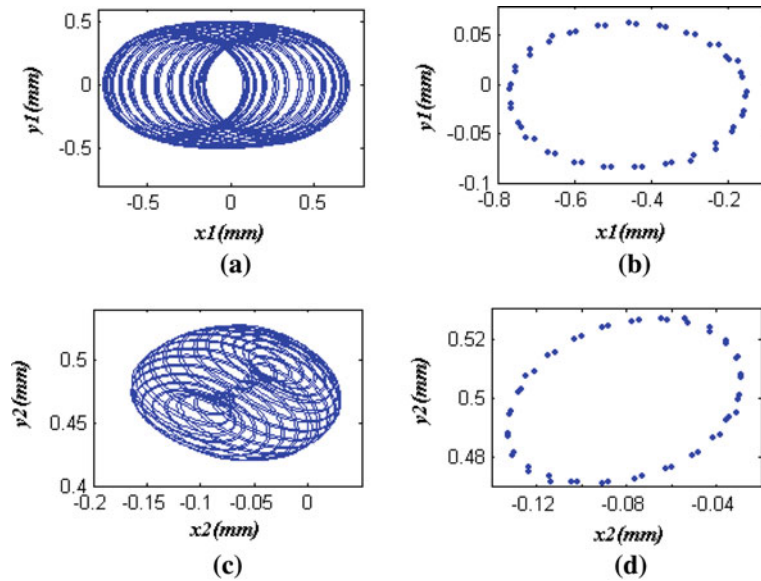
**Fig. 20** Phase plane portrait and Poincaré map of rotor center and bearing center at $\xi = 0.35$. **a** Phase plane portrait of rotor center. **b** Poincaré map of rotor center. **c** Phase plane portrait of bearing center. **d** Poincaré map of bearing center
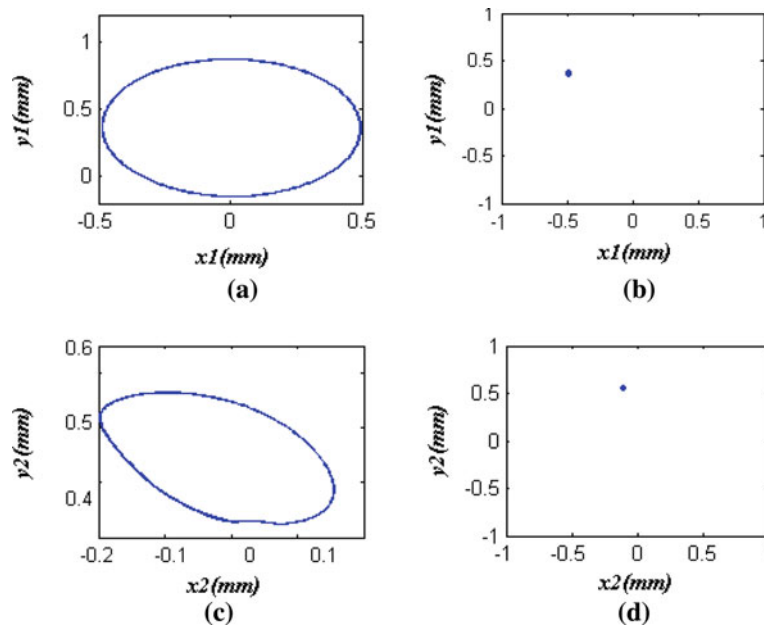
of the attractor are decomposed and finally converge to one point. Once damping ratio exceeds 0.35, the synchronous motion with period-one can be observed as displayed in Fig. 20.

Therefore, the existence of damping has a certain effect on dynamic characteristics of the rotor-bearing system. It is indicated that increasing damping can effectively suppress chaotic vibration.

## 5 Conclusions

The effects of the change in the rotating speed and damping ratio on the dynamic characteristics of the rotor system with rub-impact and oil film journal bearings are studied theoretically in detail. Due to the nonlinearity of the oil film force, computational methods have been employed to study the dynamical behavior of the system. Results of numerical calculation in horizontal and vertical directions are given and plotted via phase plane portraits, Poincaré maps, vibration responses, and the power spectrums for different system parameters. At the same time, the motion stability of the system is also investigated by numerical methods based on the Floquet theory. For the presented system, the stability analysis indicates that there exist stable periodic motions in a large range of rotating speed; however, the rotor system is unstable and shows period-doubling bifurcations in some range of rotating speed.

The main results show that the responses of the system alternate among synchronous motion with period-one, multi-periodic, chaos, and quasi-periodic motions as the rotating speed increases. On the other hand, the numerical results also indicate that the rub-impact force is the main infected factor to the response of the system along with the increase of rotating speed. Since rub-impact is transient in nature, it gives broadband excitation and the spectrum of the rub signals shows numerous spectral lines. The results also show that increasing damping can effectively restrain chaotic motion and improve the system stability. The results developed in this study allow suitable system parameters to be specified such that the rotor center and the bearing center can avoid some undesirable vibration behaviors in these types of rotating systems, hence increasing the system lives.

## References

1.  Ehrich, F.F.: Some observations of chaotic vibration phenomena in high-speed rotor dynamics. J. Vib. Acoust. **113**(1), 50–57 (1991)
2.  Li, G.X., Paidoussis, M.P.: Impact phenomena of rotor-casing dynamical-systems. Nonlinear Dyn. **5**(1), 53–70 (1994)
3.  Muszynska, A., Goldman, P.: Chaotic responses of unbalanced rotor/bearing/stator systems with looseness rubs. Chaos Solitons Fractals **5**(9), 1683–1704 (1995)
4.  Adiletta, G., Guido, A.R., Rossi, C.: Nonlinear dynamics of a rigid unbalanced rotor in journal bearings. 1. Theoretical analysis. Nonlinear Dyn. **14**(1), 57–87 (1997)
5.  Chu, F., Zhang, Z.: Bifurcation and chaos in a rub-impact Jeffcott rotor system. J. Sound Vib. **210**(1), 1–18 (1998)
6.  Dai, X., Jin, Z., Zhang, X.: Dynamic behavior of the full rotor rubbing: numerical simulation and experimental verification. J. Sound Vib. **251**(5), 807–822 (2002)
7.  Lu, Q.S., Li, Q.H., Twizell, E.H.: The existence of periodic motions in rub-impact rotor systems. J. Sound Vib. **264**(5), 1127–1137 (2003)
8.  Chu, F.L., Lu, W.X.: Experimental observation of nonlinear vibrations in a rub-impact rotor system. J. Sound Vib. **283**(3–5), 621–643 (2005)
9.  Luo, Y.G., Ren, Z.H., Ma, H., Yu, T., Wen, B.C.: Stability of periodic motion on the rotor-bearing system with coupling faults of crack and rub-impact. J. Mech. Sci. Technol. **21**(6), 860–864 (2007)
10. Shen, X.Y., Jia, J.H., Zhao, M.: Nonlinear analysis of a rub-impact rotor-bearing system with initial permanent rotor bow. Arch. Appl. Mech. **78**(3), 225–240 (2008)
11. Yuan, Z.W., Wang, S.B., Yue, X.M., Li, Z.N., Chu, F.L.: Dynamic analysis of rotor's radial rub-impact in full degrees of freedom accounting for turborotor's non-linear clearance-excitation force, Proceedings of the Institution of Mechanical Engineers, Part C. J. Mech. Eng. Sci. **222**(C9), 1647–1653 (2008)
12. Zhang, W.M., Meng, G., Chen, D., Zhou, J.B., Chen, J.Y.: Nonlinear dynamics of a rub-impact micro-rotor system with scale-dependent friction model. J. Sound Vib. **309**(3–5), 756–777 (2008)
13. Chang-Jian, C.W., Chen, C.K.: Nonlinear analysis of a rub-impact rotor supported by turbulent couple stress fluid film journal bearings under quadratic damping. Nonlinear Dyn. **56**(3), 297–314 (2009)
14. Chang-Jian, C.W., Chen, C.K.: Couple stress fluid improve rub-impact rotor-bearing system—nonlinear dynamic analysis. Appl. Math. Model. **34**(7), 1763–1778 (2010)
15. Wang, C.C.: Bifurcation and nonlinear analysis of a flexible rotor supported by a relative short spherical gas bearing system. Commun. Nonlinear Sci. Numer. Simul. **15**(9), 2659–2671 (2010)
16. Khanlo, H.M., Ghayour, M., Ziaei-Rad, S.: Chaotic vibration analysis of rotating flexible continuous shaft-disk system with a rub-impact between the disk and the stator. Commun. Nonlinear Sci. Numer. Simul. **16**(1), 566–582 (2011)
17. Adiletta, G., Guido, A.R., Rossi, C.: Chaotic motions of a rigid rotor in short journal bearings. Nonlinear Dyn. **10**(6), 251–269 (1996)
18. Han, Q.K., Zhang, Z.W., Liu, C.L., Wen, B.C.: Periodic motion stability of a dual-disk rotor system with rub-impact at fixed limiter. Vibro-Impact Dyn. Ocean Syst. Rel. Probl. **44**, 105–119 (2009)
19. Lu, Y.J., Liu, H., Dai, R., Zhang, Y.F., Yu, L., Yu, Y.B.: A method for determining the periodic solution and its stability of non-linear bearing-rotor system based on observed states of the system. Proc. Inst. Mech. Eng. Part J: J. Eng. Tribol. **223**, 137–149 (2009)